Carbohydrate Research, 229 (1992) 245–269
Elsevier Science Publishers B.V., Amsterdam

NMR spectroscopy and conformational analysis of substituted 1,2:5,6-di-*O*-isopropylidene-α-D-allofuranose derivatives

David C. Lankin [a], Sean T. Nugent [b] and Shashidhar N. Rao [c]

[a] *Physical Methodology Department,* [b] *Chemistry Department,* [c] *Drug Design, Searle Research and Development, 4901 Searle Parkway, Skokie, Illinois 60077 (USA)*

(Received August 19th, 1991; accepted in revised form December 31st, 1991)

ABSTRACT

We have utilized contemporary multidimensional NMR techniques to establish stereochemical and conformational relationships in two cyano-containing furanoses. Concurrently, theoretical calculations were performed on these two compounds using computer-assisted model building (MacroModel) and molecular mechanics (MM2). From the NOE and *J*-coupling constraints obtained from NMR experiments coupled with the results of our theoretical calculations, refined structures for these compounds have been identified and optimized. This study further highlights the significance of combining the results of NMR investigations concurrently with computational approaches in the elucidation of molecular structure in solution.

INTRODUCTION

O-Isopropylidene-D-hexofuranoses are important synthetic intermediates in modern organic chemistry[1] and, as a result, interest in the structural and conformational aspects of this general class of carbohydrates has been the subject of numerous NMR studies[2]. As part of our program to explore the use of these furanoses as chiral templates, the absolute stereochemistry of the reduction product of a 3-(cyanomethylene)furanose was required. A number of investigations have been reported on the correlation of NMR parameters with the results of molecular modeling of sugars. However, to our knowledge there have been no detailed reports wherein 2D NMR experiments coupled with molecular-modeling studies have been employed in the assignment of the stereochemistry of products in the *O*-isopropylidene-D-hexofuranoses. We report here the unequivocal assignment of stereochemistry in 3-(cyanomethylene)-3-deoxy-1,2:5,6-di-*O*-isopropylidene-α-D-ribohexofuranose (**3**) and 3-(cyanomethyl)-3-deoxy-1,2:5,6-di-*O*-isopropylidene-α-D-allofuranose (**5**) using both NMR spectroscopy and molecular-modeling techniques. The results provide very good qualitative agreement between the

Correspondence to: Dr. D.C. Lankin, Physical Methology Department, Searle Research and Development, 4901 Searle Parkway, Skokie, IL 60077, USA.

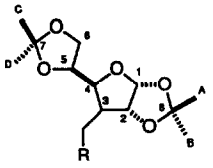

A

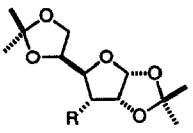

5: R = CH_2CN

6: R = H

7: R = CH_3

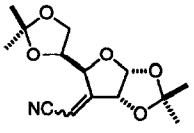

3 = E

4 = Z

NMR coupling constants and NOE values on the one hand and the independently evaluated energy-refined models on the other.

In this discussion, we have employed the standard numbering scheme to describe the substituted furanoses A. In addition we have designated the isopropylidene quaternary carbons, to which the methyl groups are attached, as C-7 (the free isopropylidene) and C-8 (the fused isopropylidene). Protons H-6 and H-6′ are respectively *cis* and *trans* to H-5.

RESULTS AND DISCUSSION

Synthesis. — Compounds **3** and **5** were prepared from the readily available 1,2:5,6-di-*O*-isopropylidene-α-D-glucofuranose (**1**, Scheme 1). Oxidation of **1** with pyridinium chlorochromate (PCC) in the presence of pulverized 3A molecular

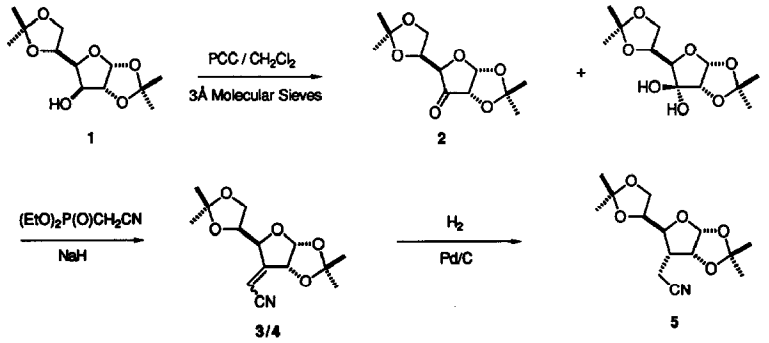

1 2 3/4 5

Scheme 1

sieves afforded a 3:2 mixture of 1,2:5,6-di-*O*-isopropylidene-α-D-*ribo*-hexofuranos-3-ulose[3] (**2**) and its hydrate. Condensation of this mixture with 2 equivalents of diethyl cyanomethylphosphonate in the presence of sodium hydride afforded, after chromatography, a mixture of the enoses[4] **3** and **4** in the ratio 9:1 (*E*/*Z*) in 70% yield. Catalytic hydrogenation of this mixture in ethyl acetate using 5% Pd–C afforded the desired cyanomethyl compound[3,4] **5** in 98% yield as a single product.

NMR studies. — The strategy employed for assignment of the proton and carbon-13 chemical shifts for the major isomeric cyano sugar **3**, and its reduction product **5**, made extensive use of contemporary 2-dimensional NMR techniques. While partial proton NMR assignments have previously been reported[4] for **3** and **5**, total unambiguous assignments of both their proton and carbon-13 NMR spectra have not. The chemical shifts (H-1, H-2, H-3′, and H-4) and coupling constants ($J_{1,2}$, $J_{2,4}$, $J_{2,3'}$ and $J_{3',4}$) obtained for **3** at 400 MHz are essentially identical to the values obtained at 100 MHz and reported earlier[4]. In the case of $J_{4,5}$, however, we clearly observe a coupling of 8.2 Hz, whereas the earlier report[4] cites an *estimated* coupling constant of 7.7 Hz. Failure to completely resolve this coupling may be attributed to possible line-broadening effects and/or non-first order behavior experienced at the lower field-strength. The assignment of the proton spectra for **3** and **5** follows from the interpretation of the phase-sensitive double quantum homonuclear shift correlation (DQF-COSY) experiment[5] as well as a phase-sensitive nuclear Overhauser homonuclear correlation spectroscopy (NOESY) experiment[6]. Figs. 1–3 summarize the homonuclear 2D NMR results. The combined use of these two 2D NMR techniques provides the necessary information which leads to a self-consistent assignment of all of the proton chemical shifts for **3** and **5**. Tables I and II summarize the proton chemical shifts and coupling constants, respectively. The assignments of the respective geminal methyl pairs in the individual isopropylidene groups present in both **3** and **5** were obtained from the DQF-COSY data. The expansion of the methyl region of **3** (Fig. 4) shows cross-peaks arising from the spin–spin coupling of the two isolated methyl pairs chemically bound to the same isopropylidene quaternary center. Similar information was extracted from the DQF-COSY data obtained for **5**, which enabled the assignment of these corresponding geminal methyl pairs to be made.

Once the geminal methyl pairs were identified, complete assignment of the individual methyl resonances could be made. For example, in the NOESY spectrum obtained for **3** (Fig. 1), cross-peaks arising from dipolar interaction of the methyl protons with the ring protons results in a self-consistent assignment of all four methyl resonances. Thus, the resonance assigned to Me(A) shows cross-peak intensities to the resonances assigned to the ring protons H-1 and H-2. The methyl resonance assigned to Me(B) exhibits only one cross-peak to the resonance assigned to H-4. The proton resonance assigned to Me(C) shows cross-peak intensities to H-5 and H-6, indicating that both are *cis* to Me(C). The resonance assigned to Me(D) shows cross-peaks to H-6′ and H-4.

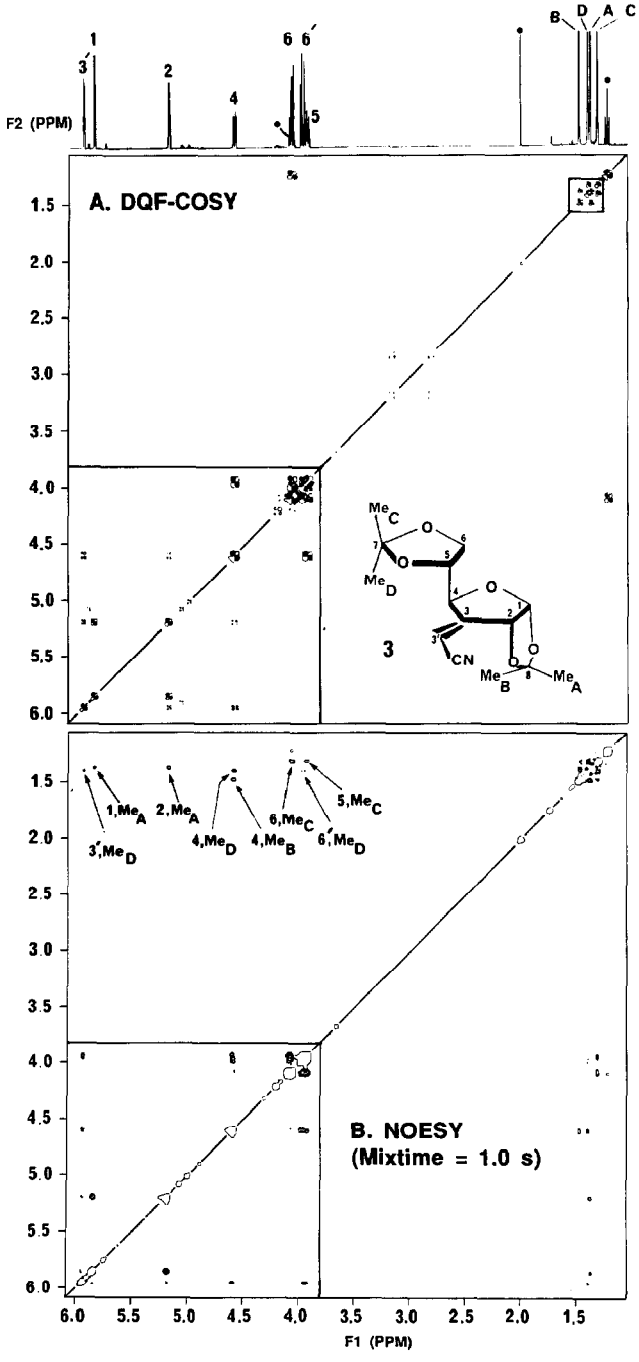

Fig. 1. (A) Phase-sensitive DQF-COSY and (B) phase-sensitive NOESY spectra for **3**. The impurity, denoted by (•) in (A), is ethyl acetate. Positive contours are plotted with full (10) contours (dark); negative contours are plotted as a single contour (open circles).

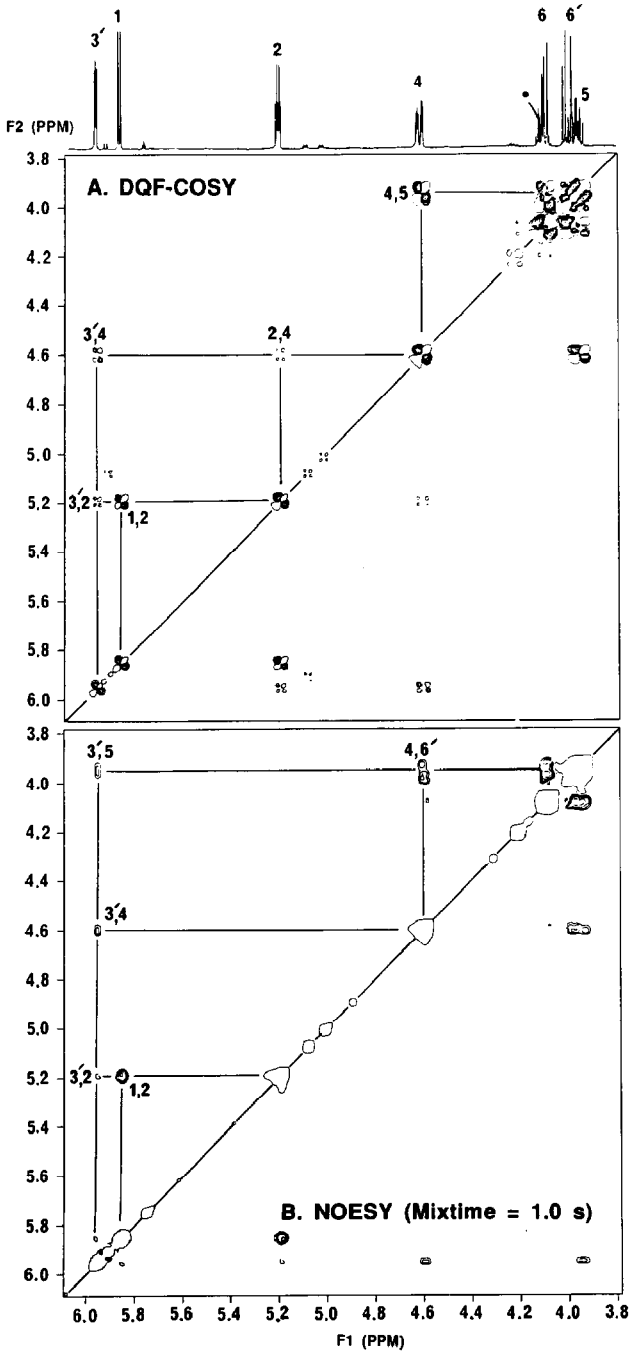

Fig. 2. Expansions (3.8–6.1 ppm) of the phase-sensitive DQF-COSY data (A) and phase-sensitive NOESY data (B) in Fig. 1.

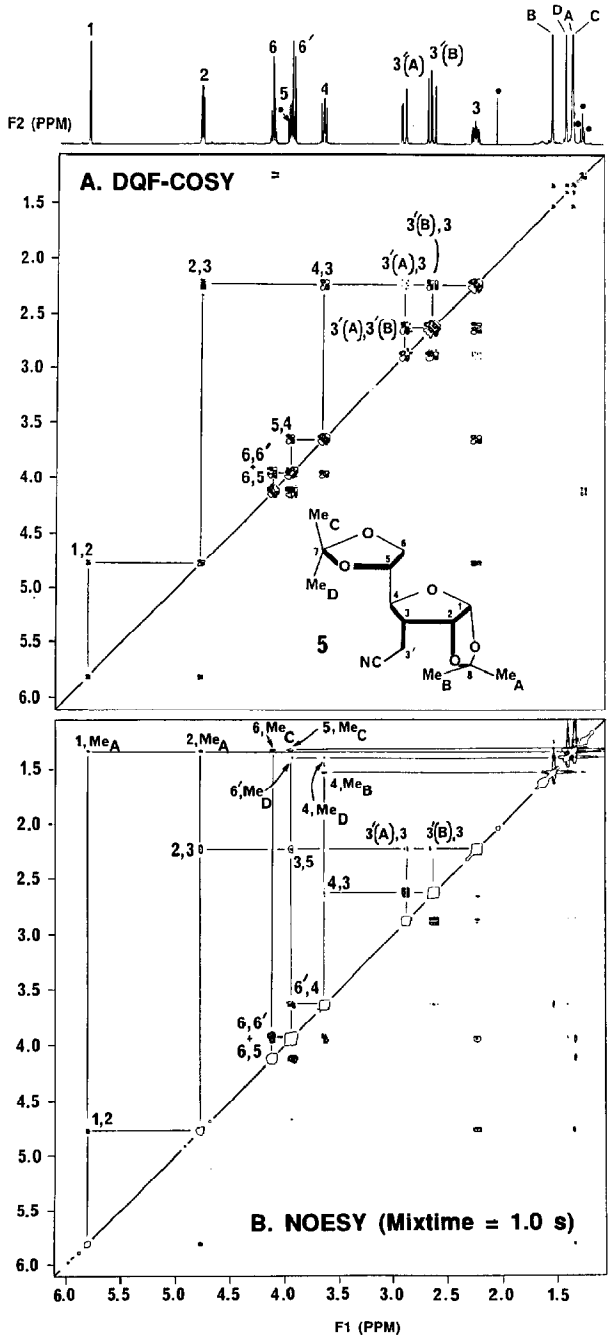

Fig. 3. (A) Phase-sensitive DQF-COSY and (B) phase-sensitive NOESY spectra for **5**. The impurity, denoted by (•), in (A) is ethyl acetate. Positive contours are plotted with full (10) contours (dark); negative contours are plotted as a single contour (open circles).

TABLE I

Proton (400 MHz) chemical-shift data [a]

Proton assignments	3	5
H-1	5.861	5.813
H-2	5.201	4.776
H-3		2.236
H-3′	5.960	
H-3′ (A)		2.826
H-3′ (B)		2.636
H-4	4.607	3.646
H-5	3.948	4.126
H-6	4.091	4.126
H-6′	3.990	3.931
Me (A)	1.387	1.349
Me (B)	1.490	1.537
Me (C)	1.324	1.340
Me (D)	1.412	1.408

[a] Chemical shifts are expressed in ppm relative to tetramethylsilane ($Me_4Si = 0.00$ ppm) used as the internal standard. Assignments were confirmed by 2-dimensional NMR experiments (DQF-COSY and NOESY).

Similarly for **5**, the methyl resonance assigned Me(A) only shows cross-peak intensities to the resonances assigned to the ring protons H-1 and H-2 indicating a *cis* relationship. The methyl resonance assigned Me(B) exhibits a cross-peak to the resonance assigned H-4. The proton resonance assigned to Me(C) shows cross-peaks to the H-5 and H-6 resonances indicating a *cis* relationship. The resonance assigned to Me(D) shows cross-peaks to H-6′ and H-4. In this way, by identifying the respective geminal pairs of methyl groups (DQF-COSY) and then evaluating

TABLE II

Summary of proton–proton coupling constants [a]

Proton assignments	3	5
$J_{1,2}$	4.0	3.8
$J_{2,3}$		4.6
$J_{2,3'}$	1.5	
$J_{2,4}$	1.4	
$J_{3,3'(A)}$		3.7
$J_{3,3'(B)}$		11.2
$J_{3'(A),3'(B)}$		−16.6
$J_{3',4}$	2.2	
$J_{3,4}$	9.7	
$J_{4,5}$	8.2	8.2
$J_{5,6}$	6.1	5.8
$J_{5,6'}$	4.6	5.0
$J_{6,6'}$	−8.8	−8.4

[a] Coupling constants are expressed in Hz. The sign of the geminal coupling constants is inferred.

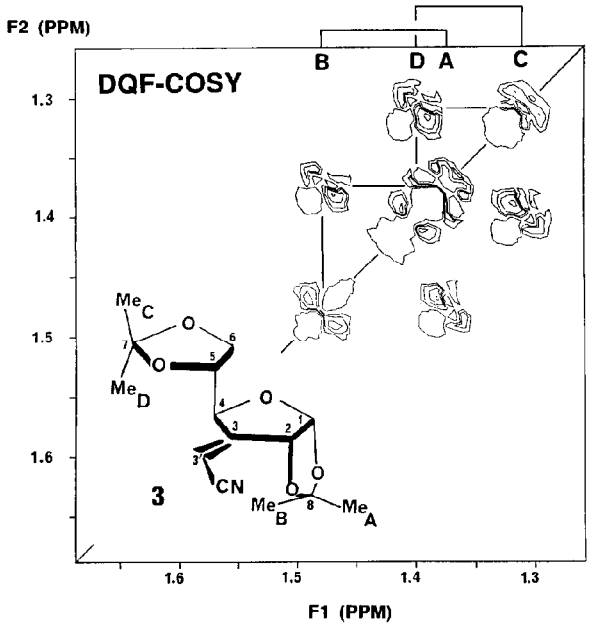

Fig. 4. Expansion of the geminal dimethyl region of the DQF-COSY spectrum (A) in Fig. 1 fo 3.

the dipolar interactions via the NOE values of the methyl groups with the ring protons (NOESY), a self-consistent set of proton assignments is obtained for both **3** and **5**.

The assignment of the carbon-13 spectra for **3** and **5** follows after an initial determination of thc carbon-13 resonance multiplicities using the attached proton test (APT) experiment[7]. Subsequent assignment of the respective protonated carbons was derived from the results of the 2-dimensional heteronuclear proton–carbon shift correlation (HETCOR)[8] spectra for **3** and **5**. This approach leads to an unambiguous assignment of their respective protonated carbon resonances. Figs. 5 and 6 show the results of the HETCOR experiments obtained for **3** and **5**.

The assignment of the isopropylidene quaternary carbons in **3** and **5** was made in a straightforward manner using single-frequency selective decoupling of the geminal dimethyl protons in **3** and **5**, while observing the carbon-13 spectra, and correlating these results with the previously reported[9] carbon-13 assignments which arc based upon the isopropylidene acetal ring size. Fig. 7 summarizes the carbon-13 NMR assignments for **3** and **5**. The assignments of the isopropylidene quaternary carbons made here are consistent with the data previously reported[2,9,10] for related isopropylidene acetals.

With the proton and carbon-13 spectra for **3** and **5** fully assigned, attention was focused on the stereochemistry of the C – 3 substituent in these compounds.

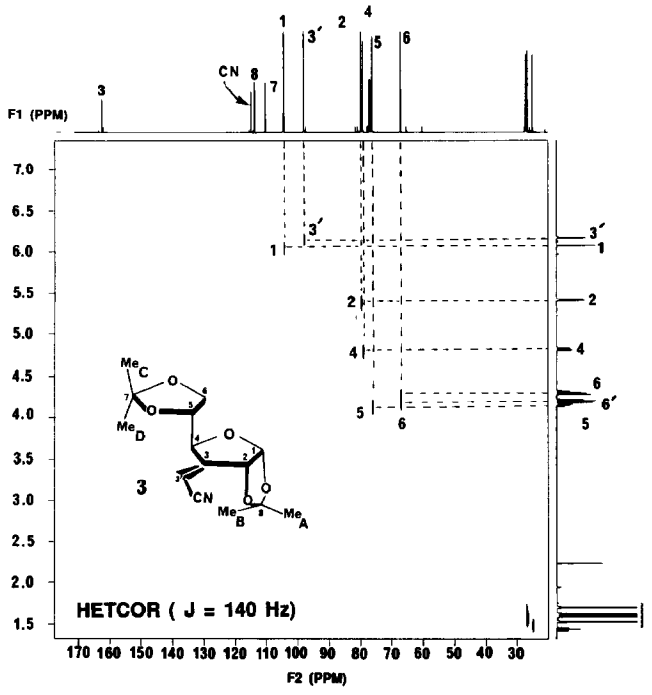

Fig. 5. The proton–carbon-13 heteronuclear shift correlation (HETCOR) for **3**.

Assignment of stereochemistry in **3** (Z vs. E) follows from the analysis of its NOESY spectrum (Figs. 1 and 2). In this study, NOE intensities are arbitrarily assigned as "strong", "medium", and "weak" and correspond to distance ranges of 1.8–2.0, 2.0–3.0, and 3.0–4.0 Å, respectively. NOE intensities not observed correspond to distances > 4.0 Å. The relative intensities of NOESY cross-peaks were evaluated from the 2D contours based on visual comparisons of the intensities of the geminal and vicinal NOESY cross-peaks relative to the longer range cross-peaks. We also examined the intensity information obtained from slices of the NOESY contour plots. The observed NOE to Me(A) and Me(B) correspond to their average positions consistent with rapid rotation about the appropriate C–C bond. The NOESY data for **3** indicates cross-peaks correlating the vinyl proton H-3′ to the proton H-2 (weak) as well as to protons H-4 and H-5 (both medium) which is consistent with the indicated (namely E) stereochemistry assigned to **3**. The stereochemistry at C-3 in **5** ($R + \alpha$ vs. $S = \beta$) is based on the interpretation of the NOESY spectrum obtained for **5** (Fig. 3) which indicates a family of cross-peak correlations between H-3 and H-2 as well as between H-3 and H-5. These cross-peaks establish that H-3 is *syn* to H-2 and spatially proximate to H-5. Additionally, H-3′(B) shows a cross-peak correlating to H-4. This cross-peak can only be present if the cyanomethyl moiety is *trans* to H-2 and *cis* to H-4. Further, only weak cross-peaks are observed between H-3 and H-3′(A) and H-3′(B)

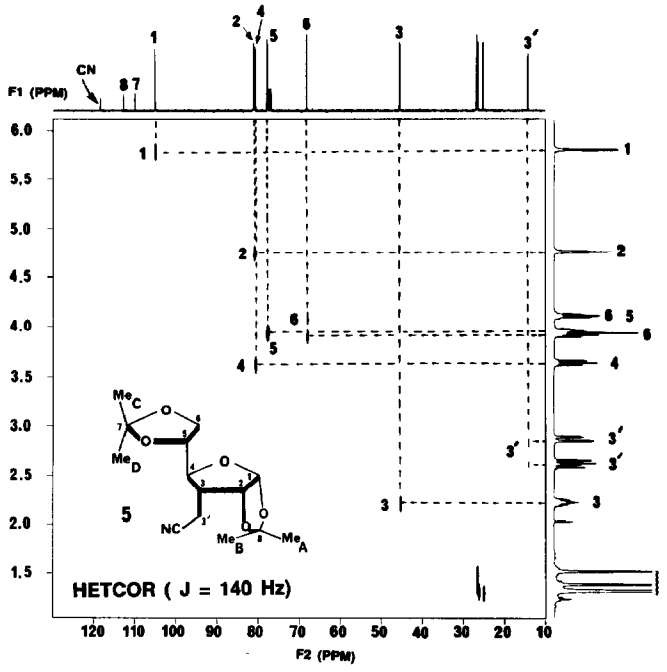

Fig. 6. The proton–carbon-13 heteronuclear shift correlation (HETCOR) for **5**.

indicating that these protons must be pointing away from H-3. Thus, C-3 of **5**, consistent with the observed NOESY data, possesses the *R* configuration indicating that catalytic reduction of **3** to **5** proceeds with delivery of hydrogen to the β face of the double bond consistent with previously reported results[4].

Molecular modeling. — Concurrent with the NMR studies, four derivatives of the allofuranoses (**3**, **5**, **6**, and **7**) were investigated by molecular mechanics. The calculated conformations obtained at two dielectric values (1.0 and 10.0) are

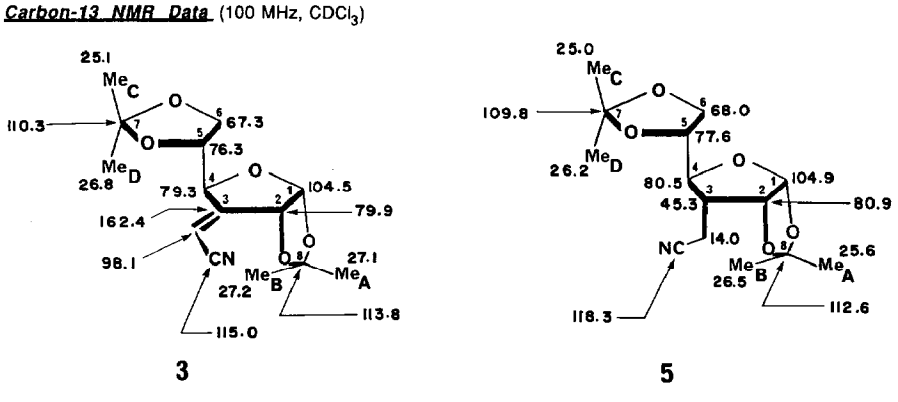

Fig. 7. Carbon-13 NMR data for cyano sugars **3** and **5**.

TABLE III

Torsion angles in the ten best energy-refined structures of **3** (a) and **5** (b). Corresponding torsions for torsions for **7** are shown in parentheses in (b)

(a)

	H-1-C-1-C-2-H-2	H-2-C-2-C-3-H-3	H-3-C-3-C-4-H-4	H-4-C-4-C-5-H-5	H-3-C-3-C-3′-H-3′	H-3-C-3-C-3-H-3″
a	1.1			55.8		
b	1.9			55.5		
c	0.4			170.9		
d	0.1			172.6		
e	0.2			−72.9		
f	0.6			179.5		
g	0.4			178.7		
h	0.7			−67.4		
i	1.4			−64.7		
j	3.9			55.8		

(b)

	H-1-C-1-C-2-H-2	H-2-C-2-C-3-H-3	H-3-C-3-C-4-H-4	H-4-C-4-C-5-H-5	H-3-C-3-C-3′-H-3′(A)	H-3-C-3-C-3′-H-3′(B)
a	−7.1 (−6.7)	39.6 (37.2)	−168.5 (−166.0)	179.3 (181.0)	55.1	174.9
b	−5.8 (−6.7)	39.8 (37.2)	−170.3 (−166.1)	181.2 (179.7)	−70.2	47.1
c	−7.1 (−6.9)	39.6 (36.0)	−168.7 (−166.5)	177.2 (−62.2)	55.6	175.3
d	−7.1 (−6.7)	39.8 (37.2)	−169.2 (−166.3)	176.4 (179.3)	54.7	174.4
e	−7.3 (−6.5)	40.1 (36.4)	−170.7 (−165.7)	177.9 (64.3)	160.2	−80.9
f	−5.9 (−6.8)	40.1 (36.9)	−171.2 (−166.3)	179.2 (62.6)	−71.4	46.1
g	−7.3 (−6.8)	40.3 (36.2)	−171.3 (−166.4)	173.6 (−62.9)	161.0	−80.0
h	−7.3 (−7.5)	39.8 (−6.9)	−170.5 (−96.0)	177.5 (−66.9)	161.3	−79.7
i	−7.6 (−8.0)	39.9 (−7.2)	−172.9 (−93.8)	−75.7 (177.3)	55.7	175.7
j	−7.0 (−6.8)	38.9 (−7.0)	−168.3 (−97.7)	63.8 (−66.8)	57.7	−177.1

practically identical. This is not surprising in light of the fact that in this series no intramolecular electrostatic stabilizations are feasible. Hence, the following discussions will be confined to the variations in the models obtained with a dielectric value of 1.0. The terms "around" and "approximately" used herein refer to deviations of no more than 0.1 Å in the case of measured distances and more than 10% in the case of torsion angles.

Table III lists the torsion angles which can be correlated with the observed *J*-coupling results (Table II) for the top ten energy-minimized structures of **3**, **5**, and **7**, starting from the respective global minimum. The torsion angles for **6** are not listed as they are practically identical to those of **5**. The corresponding energies relative to that of the global minimum structure for each of the four compounds are listed in Table IV. The ten models will be referred to with suffixes **a** through **j** in the following text. The highest energy local minima of **3**, **5**, **6**, and **7** are destabilized relative to the respective global minima by 3.7, 6.7, 5.2 and 6.0 kcal/mol, respectively. The number of models within 1 kcal/mol of the global minimum ranges from 3 models for **6** to 8 models for **3** (Table IV). While for **3** and

TABLE IV

Energies (in kcal/mol) relative to global minimum of ten best energy-minimized structures of **3**, **5**, **6**, and **7** whose conformations are listed in Table III and discussed in the text

	3	**5**	**6**	**7**
a	0.00	0.00	0.00	0.00
b	0.44	0.37	0.62	0.70
c	0.50	0.49	0.71	0.77
d	0.52	0.76	1.27	0.81
e	0.53	0.76	1.32	1.32
f	0.69	0.86	1.44	1.53
g	0.89	1.37	2.60	1.57
h	0.91	1.52	3.89	3.41
i	1.10	1.55	5.20	4.29
j	1.30	1.95		4.56

5, the ten best models lie within 2 kcal/mol of the respective global minima, for the other two compounds they span a wider energy-range (Table IV).

Computer graphic illustrations of the global minimum conformations and of minima that lie within 0.5 kcal/mol of the global minima are shown in Figs. 8 and 9 for **3** and **5**, respectively. In the case of **3**, the global minimum is not entirely consistent with the observed NMR data, while in the case of **5**, global minimum and three other minima (**5b**, **5c**, and **5d**) within 1 kcal/mol of the former are consistent with the NMR results. An overlap of the global minimum of **5** with two minima of **3**, all of which are consistent with the observed coupling constants and NOE values, is shown in Fig. 10.

Protons H-1 and H-2 are very nearly eclipsed with the torsion angle about the C-1–C-2 bond being around $-7°$ in all of the energy optimized structures (Table III). In **3**, this torsion angle has values closer to $0°$ ($1 \pm 1°$), while in **6** and **7**, it has values around $-7°$ as in **5** (Table V).

The coupling constants obtained from our NMR studies for protons H-1 and H-2 are around 4.0 Hz (Table II). Using a refinement of the original[11] Karplus relationship, namely, that of Hasnoot and coworkers[12], the coupling constants for H-1 and H-2 were calculated to be ~ 5.7 Hz for **5** and 6.0 Hz for **3**. While absolute values of these calculated couplings are high and deviate from the experimentally observed coupling constants by nearly 2 Hz, their calculated difference (~ 0.3 Hz) is closely comparable to the experimentally observed difference (0.2 Hz).

The dihedral angle H-2–C-2–C-3–H-3 is around $40 \pm 0.5°$ in all of the energy-refined models of **5** and **7**. However, in **6**, this torsion angle attains two sets of values. In the first set, they are $\sim 40°$ as in **5** and **7**, while in the second set, they are around $-7°$. Correspondingly, the second proton at C-3 in **6** has torsion angles of around $-85°$ and $-128°$, respectively. The first set of structures include the global minimum and minima which are within 1.6 kcal/mol of the global mini-

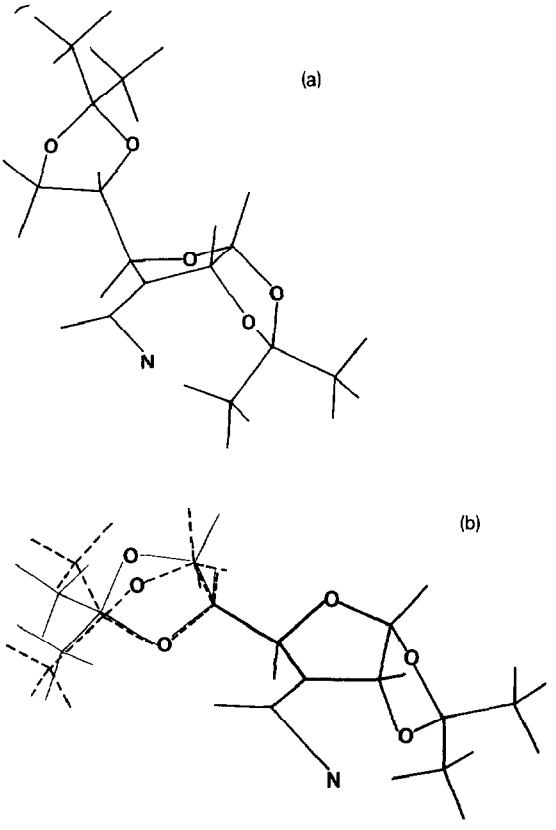

Fig. 8. Computer graphic representations of **3a** (a) and an overlap of **3b** (dashed line) and **3c** (thin solid line). Solid dark lines indicate exact conformational overlap.

mum. The structures in the second set are destabilized by 3.4–6.0 kcal/mol relative to the global minimum.

The observed coupling between H-2 and H-3 is 4.6 Hz in **5** (Table II) and the

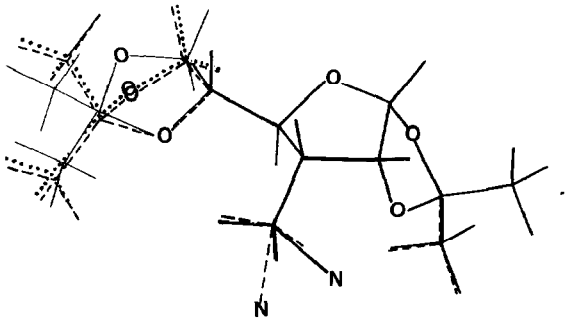

Fig. 9. Computer graphic representation of **5a** (dotted line) overlapped with two minima within 0.5 kcal/mole of the global minimum, **5b** (dashed line) and **5c** (thin solid line). Solid dark lines indicate exact conformational overlap.

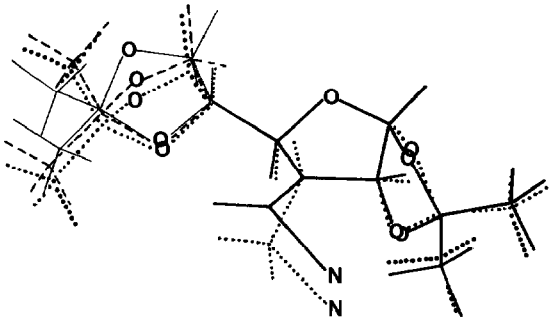

Fig. 10. Overlap of **5a** (dotted line) with **3b** (dashed line) and **3c** (thin solid line). Solid dark lines indicate exact conformational overlap.

corresponding calculated value[12] is ~ 5.0 Hz. In the NMR investigations reported[13] for **6**, the coupling constants between H-2 on the one hand and the two protons at C-3 on the other were observed to be ~ 4.8 and 0.4 Hz. These data were interpreted in terms of torsion angles of 14 and 110°, respectively[11]. These values differ significantly from those in the energy-refined models obtained in the present study (Table III). In fact, the calculated coupling constants[12] for H-2 and H-3 in

TABLE V

Torsion angles describing the 5,6-isopropylidene ring in the ten best energy-minimized models of **3** (a) and **5** (b)

	H-5–C-5–C-6–H-6	H-5–C-5–C-6–H-6′	C-6–C-5–O-5–C-7
(a)			
a	4.2	129.0	−29.3
b	−7.4	117.0	−18.9
c	3.8	128.1	−27.8
d	43.5	170.0	−34.7
e	−8.7	115.7	−17.6
f	27.0	152.6	−1.9
g	2.9	127.7	−28.0
h	3.8	128.3	−27.5
i	3.4	128.1	−28.3
j	31.9	157.9	−7.6
(b)			
a	3.1	127.8	−28.1
b	1.1	125.9	−26.5
c	43.5	170.2	−33.3
d	25.4	150.9	0.7
e	3.8	128.6	−29.0
f	23.6	149.0	3.1
g	43.7	170.0	−37.7
h	23.7	149.0	2.8
i	−1.6	122.7	−23.7
j	5.1	129.7	−28.5

energetically favored models (which lie within 1.5 kcal/mol of the global minimum) are ~5.0 Hz, within 0.3 Hz of the experimental value. We calculated[12] a corresponding coupling of 9.7 Hz in a model with the dihedral angles reported earlier[13].

Interestingly our studies *not only* demonstrate that the energetically favored models are nearly quantitatively and qualitatively consistent with the observed NMR coupling constants in the case of **6**, but provide an alternative structural interpretation for the previously reported NMR data[13]. The observed coupling constant between H-2 and H-3 in the NMR studies on **7** reported earlier[19a] is 3.7 Hz. This value is lower than both the calculated coupling constants derived from the energy-minimized models of **7** (~5.0 Hz) and the corresponding coupling constants observed here for **5** (Table II) as well as **6** reported earlier[13]. The value of the coupling constant $J_{2,3}$ which we have observed for **5** (4.6 Hz) is also higher than that previously reported[3] for **5** (3.6 Hz), but is in better accord with the value calculated from the refined models (see above).

The torsion angle H-4–C-4–C-3–H-3 is predominantly around −170° in **5** and **7**, consistent with the observed coupling constant of 9.7 Hz. In **6**, this torsion angle adopts two sets of values for each of the two protons at C-3 (Table III). The first set, which includes structures within 1.6 kcal/mol of the global minimum, has these torsion angles around 194 and −43°. The second set, which consists of structures more than 3.5 kcal/mol relative to the global minimum, has these torsion angles around −95 and 25°. These torsion-angle pairs correspond to calculated coupling constants of 11.5 and 4.5 Hz (first set) and 1.6 and 8.7 Hz (second set), respectively. The observed coupling constants for the two protons at C-3 and H-4 are ~10.0 and 3.9 Hz, respectively[13]. This once again demonstrates that the global minimum and low-energy models within 1.5 kcal/mol of the former satisfy the experimental observations.

The torsion angle H-4–C-4–C-5–H-5 defines the orientation of the 5,6-isopropylidene ring relative to the [3.3.0] ring system. In **5**, this torsion angle is calculated to be predominantly between 175 and 180°. Very few structures have *gauche* values for this torsion angle. In **3**, **6**, and **7**, however, the torsion angles are spread over three sets of values: *anti* (~180°), *gauche*$^+$ *(55–70°) and gauche*$^-$ (−60 to −80°). Thus, it appears that introduction of a substituent at C-3 which is bulkier than a methyl group induces a conformational restriction about the C-4–C-5 bond. The coupling constants obtained from NMR measurements between these two protons is 8.2 Hz in both **3** and **5**. This suggests that for **3**, the solution structure has a torsion angle close to *anti* rather than *gauche*$^+$ as was found in the global minimum. Indeed the lowest-energy structure with an *anti* configuration about the C-4–C-5 bond is only 0.5 kcal/mol higher in energy (**3c** in Tables III and IV) than the global minimum.

In **5**, the coupling constants between H-3–H-3′(A) and H-3–H-3′(B) are 3.7 and 11.2 Hz, respectively. This implies the *gauche*$^+$ or *gauche*$^-$ conformation for H-3–H-3′(A) and an *anti* conformation for H-3–H-3′(B). In the refined models,

torsion angles about the C-3–C-3′ bond spread over the *anti* (~ 180°), *gauche*$^+$ (~ 60°) and *gauche*$^-$ (~ 60°) ranges. Consistent with this, the torsion angles H-3–C-3–C-3′–H-3′(A) and H-3–C-3–C-3′–H-3′(B) are ~ 60 and 180° in the global minimum and three other models (**5b**, **5c**, and **5d**) which are within 1 kcal/mol of the global minimum.

An interesting aspect of the structures of **3** and **5** is the geometry of the 5,6-isopropylidene ring, which we have chosen to describe in terms of two torsion angles, H-5–C-5–C-6–H-6 and C-6–C-5–O-5–C-7. The former torsion angle may be directly related to two of the measured coupling-constants, namely $J_{5,6}$ and $J_{5,6'}$. Table V lists these torsion angles for the ten best energetically favored models of **3** and **5**. The corresponding torsion angles in **6** and **7** are very similar to those in **5** and hence are not discussed. The twist forms and not the envelope forms are observed for this isopropylidene ring in all of the energy-minimized models. This observation is consistent with the published results of computational investigations on a number of furanose derivatives which indicate that twist conformations, rather than envelope forms, characterize low-energy structures[20]. For the global minimum of **3** and **5**, H-5 and H-6 are related by torsion angles around 4 and 3°, respectively. As shown in Table V, this torsion angle varies over a range of nearly 50°. The endocyclic torsion angle C-6–C-5–O-5–C-7 also varies over a nearly 40° range in both of the compounds. These variations demonstrate the flexible nature of the conformation of the 5,6-isopropylidene ring. This flexibility is qualitatively consistent with the observed coupling constants (5–6 Hz) between H-5 and H-6 (Table II). This corresponds to an interconversion of the isopropylidene ring conformations where the transition of a proton is induced between states of large (~ 0°) and small (~ 40°) *J*-coupling. Such a transition is reasonable in light of the low barriers of interconversions (~ 2–3 kcal/mol)[16] in cyclopentane and furanose rings. Hence, probing of the molecular dynamics in this instance by standard solution NMR techniques (i.e., low temperature ~ 150°) may be precluded by the practical limits of the instrumentation.

In addition to the proton–proton torsion angles, the interproton distances in the energy-optimized models may be used in identifying structures consistent with the NMR data. Only the calculated interproton distances for **3** and **5** will be discussed together with the corresponding NOE values (Table VI). The average distances in energy-refined models were computed with each of the three protons in a methyl group, and compared qualitatively with an observed NOE or lack thereof.

In the energy-refined models of **5**, the H-1–H-2 and H-2–H-3 distances are ~ 2.5 Å, consistent with the medium NOE between them. The distances between H-3–H-4 and H-4–H-5 are calculated to be ~ 3.1 Å in all of the models and are consistent with medium-to-weak NOE values observed between them. The geminal protons H-6 and H-6′ show a strong NOE cross-peak since they are separated by a distance of 1.8 Å. The H-5–H-6 distances vary between 2.3 and 2.5 Å and are consistent with the medium NOE observed.

In all of the models, the H-1(H-2) distances to Me(A) are in the range of

TABLE VI

Observed NOE data on **3** and **5** qualified as strong (s), medium (m), and weak (w)

3		**5**	
H-1 ↔ H-2	m	H-1 ↔ H-2	m
H-3′ ↔ H-2	w	H-3 ↔ H-2	m
H-3′ ↔ H-4	w	H-3 ↔ H-4	w
H-3′ ↔ H-5	w	H-5 ↔ H-4	w
H-4 ↔ Me(B)	w	H-5 ↔ H-6	m
H-4 ↔ Me(D)	w	H-4 ↔ Me(B)	w
H-6 ↔ Me(C)	w	H-3 ↔ H-3′A	w
H-5 ↔ Me(C)	w	H-3 ↔ H-3′B	w
H-4 ↔ Me(D)	w	H-4 ↔ H-3′B	w
H-3′ ↔ Me(D)	w	H-3 ↔ H-5	m
H-1 ↔ Me(A)	w	H-1 ↔ Me(A)	w
H-2 ↔ Me(A)	w	H-2 ↔ Me(A)	w
H-6 ↔ H-6′	s	H-6 ↔ H-6′	s
		H-5 ↔ Me(C)	w
		H-4 ↔ Me(D)	w
		H-6 ↔ Me(C)	w
		H-6′ ↔ Me(D)	w

3.5–4.0 Å, while the distances from H-1(H-2) to Me(B) are significantly larger than 4.5 Å. These distances are consistent with the weak NOE (Table VI) observed to Me(A) and the absence of NOE to Me(B). The models predict the distances between H-4 and Me(A) and Me(C) to be larger than 4.5 Å, consistent with the fact that no corresponding NOE are observed. The distance of H-4 to Me(B) is calculated to be 4.0 Å in all the models, corresponding to a weak NOE as observed (Table VI). The distance between H-4 and Me(D) is 4.0 Å in most of the energy-optimized models with the exception of **5e**, **5f**, and **5i** where values of 3.5 Å are calculated. Models **5e** and **5f** are within 1 kcal/mol of the calculated global minimum while **5i** is 1.6 kcal/mol above the global minimum (Table V). Interestingly, *only* in these three models are the distances between H-5(H-6) and Me(C) greater than 4.0 Å, while in all other models they vary from 3.1 to 3.4 Å. A distance of 2.5 Å between H-3 and H-5 in all of the energy-minimized models is consistent with an observed medium NOE.

The distances between H-3–H-4 and H-3′(A) and H-3′(B) are calculated to lie in the range 2.5–3.5 Å, corresponding to a medium-to-weak NOE for both. However, the experiment shows the NOE between these protons to be weak, possibly due to hindered rotation about the C-3–C-3′ bond. For example, replacement of the cyano group in **5** with a hydroxyl group introduces intramolecular hydrogen bonding to spatially proximate oxygens. This can further contribute to a restriction of rotation[17]. An *anti* conformation for either H-3′(B) or H-3′(A) relative to H-3 would lead to the lack of a NOE cross-peak between them, since the corresponding C-H vectors would be pointed in opposite directions. As noted earlier, all models within 2 kcal/mol of the global minimum (**5a**) have a range of

torsion angles about the C-3–C-3′ bond. It is, therefore, not surprising that a weak NOE is observed for one of the C-3′ protons.

In **3**, the calculated H-2–H-3′ distance lies between 3.9 and 4.0 Å, consistent with the weak NOE observed (Table VI). As in **5**, the H-1–H-2 NOE is medium as these protons are separated by ~2.5 Å in all the models. The H-4–H-3′ distance is either around 2.7 or 3.3 Å corresponding to medium or weak NOE cross-peaks. The distances of H-1 and H-2 to the Me(A) protons average about 3.3–3.5 Å, consistent with the observed weak NOE (Table VI). The calculated distances of H-4 with Me(A) and Me(C) are greater than 4.5 Å, consistent with the absence of a NOE cross-peak. However, NOE cross-peaks are observed between both Me(B) and Me(D) with H-4(Fig. 1). The distance between H-4 and Me(B) is ~4.2 Å in all of the energy-refined models of **3** except for **3b** and **3g**, where it is ~3.7 Å. These two models lie within 1 kcal/mol of the global minimum. The distances between H-4 and Me(D) are greater than 4.5 Å in all of the refined models of **3** except for **3f** where it is ~3.6 Å. The distances between H-5–Me(C) and H-6–Me(C) are in the range of 3.5–3.7 Å, consistent with the medium-to-weak NOE observed between Me(C) and the protons at C-5 and C-6. The distance between H-5 and H-3′ ranges from 2.4 to 4.4 Å with an average of 3.5 Å for the top ten energy-refined models of **3**. This is consistent with the observation of a weak NOE between these two protons. The distances between Me(D) and H-6′ are calculated to be >4.5 Å in all models except for **3d** and **3f** where they are ~3.5 Å. Thus, only the latter two models are consistent with an observed weak NOE between these two protons.

The foregoing detailed discussions on the structure and conformations of energy-refined models of **3**, **5**, **6** and **7** indicated generally very good consistency with experimental observations. It must be pointed out that for each of the compounds, no unique energy-refined structure was obtained satisfying all of the experimental data, although models which lie within 1 kcal/mol of the respective global minima do individually satisfy most of the observed NOE and *J*-couplings. Thus, it may be speculated that these compounds exist as an equilibrium mixture of conformations which are within 1.5 kcal/mol of the global minimum.

CONCLUSIONS

We have conducted a stereochemical analysis of two synthetically derived allofuranoses through the combined use of contemporary multidimensional NMR and molecular-modeling techniques. While the addition of hydrogen to the double bond in **3** can occur from either the α- or β-face leading to two possible cyanomethyl products, **5** or **epi-5**, the NMR experiments clearly confirm the product to be structure **5**. This indicates that addition of hydrogen occurs from the β-face of **3**, consistent with predictions based on steric criteria. Very good qualitative agreement was also obtained between the observed NMR *J*-couplings and NOE and the models obtained from computational methods. The molecular-mod-

cling study finds a family of low-energy models rather than a single unique model to be endowed with structural characteristics consistent with the NMR data. This study further highlights the significance of combining the results of NMR investigations concurrently with computational approaches in the elucidation of molecular structure in solution.

EXPERIMENTAL

General procedures. — All reactions were carried out at ambient temperature under an Ar atmosphere unless otherwise indicated. The term in vacuo refers to concentration first by a rotary evaporator followed by use of a vacuum pump (< 0.5 torr). Infrared spectra were recorded on a Perkin–Elmer Model 681 grating spectrophotometer (cm^{-1}) in $CHCl_3$. Mass spectra were determined on a Finnigan MAT 8430 (0.1 torr NH_3). All NMR spectra were measured in 5-mm o.d. tubes (Wilmad-535) in $CDCl_3$ (Merck Isotopes) solution at 20°.

1,2:5,6-Di-O-isopropylidene-α-D-ribo-*hexofuranos-3-ulose*[3] (**2**). — To a suspension of 12.9 g (60.0 mmol) of PCC, 12.8 g of pulverized 3A molecular sieves in 50 mL of CH_2Cl_2 was added a solution of di-*O*-isopropylidene-1,2:5,6-α-D-glucofuranose (**1** 5.20 g; 20.0 mmol) in CH_2Cl_2 (50 mL) dropwise over 45 min to the resulting dark-brown solution. The mixture was stirred for 16 h at which time 100 mL of Et_2O was added. After stirring for an additional 2 h, the mixture was passed through a column containing 150 g of silica gel topped with 50 g of Celite. Elution with Et_2O followed by concentration in vacuo afforded 4.8 g of a 1:1 mixture of ketone **2** and its corresponding hydrate (89%) as a solid: CI-MS *m/z* 276 ($M + NH_4^+$), 259 ($M + H^+$, 100%); ^{1}H-NMR: δ 6.15 (d, 1 H), 5.83 (d, 1 H), 4.5–3.8 (bm, 12 H), 1.56 (s, 3 H), 1.46 (s, 3 H), 1.43 (s, 3 H), 1.42 (s, 3 H), 1.37 (s, 3 H), 1.33 (s, 3 H), 1.30 (s, 3 H); ^{13}C-NMR: δ 208.0, 114.1, 113.1, 110.2, 109.7, 104.0, 102.8, 100.7, 83.4, 78.6, 78.5, 76.0, 73.7, 66.5, 64.0, 27.2, 26.8, 26.6, 26.3, 25.6, 25.0, and 24.8;

Anal. Calcd for $C_{12}H_{18}O_6 \cdot 0.5\ H_2O$: C, 53.93; H, 7.15. Found: C, 54.21; H, 7.39.

*3-(Cyanomethylene)-3-deoxy-1,2 : 5.6-di-*O*-isopropylidene-α*-D-ribo-*hexofuranose*[4] (**3/4**). — To a suspension of 1.65 g (41.3 mmol) of a 60% dispersion of NaH (pre-washed 4 × with hexane) in 40 mL of 1,2-dimethoxyethane cooled in an ice bath was added dropwise a solution of 6.65 g (37.6 mmol) of diethyl cyanomethylphosphonate in 10 mL of 1,2-dimethoxyethane. After 30 min a solution of 4.8 g (18.0 mmol) of **2** in 80 mL of 1,2-dimethoxyethane was added dropwise. The reaction was stirred at room temperature for 16 h at which time 100 mL of water was added and the layers separated. The aqueous layer was extracted twice with CH_2Cl_2, the organic material combined and washed with brine, dried ($MgSO_4$), and concentrated in vacuo. Purification by column chromatography (silica gel, 20% EtOAc–hexane) afforded 3.53 g (70%) of a mixture of **3** and **4** (9:1) as a pale-yellow liquid: $[\alpha]_D^{25}$ +131.4° (*c* 0.9, $CHCl_3$); IR 3010, 2990, 2940, 2880, and 2230 cm^{-1}; CI-MS *m/z* 299 ($M + NH_4^+$), 282 ($M + H^+$); ^{1}H-NMR data are

summarized in Tables I and II and Figs. 1, 2, and 4; ^{13}C-NMR data are summarized in Fig. 7.

*3-(Cyanomethyl)-3-deoxy-1,2:5,6-di-*O*-isopropylidene-α-*D*-allofuranose*[3,4] (**5**): — The foregoing mixture (557 mg, 1.98 mmol) was dissolved in 25 mL of EtOAc and 56 mg of 5% Pd–C added. This was placed on a Parr shaker apparatus and hydrogenated at atmospheric pressure (25°) for 135 min. The catalyst was filtered and the solvent removed by rotary evaporation. The residue was taken up in 50 mL of EtOAc, filtered through Celite and concentrated in vacuo affording 551 mg (98%) of **5** as a white solid: $[\alpha]_D^{25}$ +73.2° (*c* 0.895, $CHCl_3$) (lit.[3a] $[\alpha]_D^{22}$ +91° (*c* 2, $CHCl_3$)); mp 104–106° (lit.[3a] mp 109°); IR 2950, 2255 cm^{-1}; CI-MS *m/z* 301 ($M + NH_4^+$), 284 ($M + H^+$); ^{1}H-NMR data are summarized in Tables I and II and Fig. 3; ^{13}C-NMR data are summarized in Fig. 7.

NMR spectroscopy. — One-dimensional ^{1}H- and ^{13}C-NMR spectra were collected on either a Varian VXR-400 spectrometer operating at 400 and 100 MHz, respectively, or a General Electric QE-300 instrument operating at 300 and 75 MHz, respectively. All two-dimensional NMR spectra were collected on the VXR-400 instrument, which was equipped with a 5-mm BB switchable probe and variable-temperature accessory.

Phase-sensitive double quantum filtered COSY. — The experimental conditions for **3** were as follows: sequence, D1–(90)–t_1–(90)(90)–acquire (t_2); relaxation delay (D1) = 11 s; PW90 = 25.5 μs; acquisition time (AT) = 344 ms; spectral window (SW) = 2976.2 Hz; the number of data points (NP) in F_2 was 2048 and the number of increments (NI) = 2 × 256, employing the States–Haberkorn–Ruben[8] hypercomplex data-collection and data-processing scheme; the number of transients/increment (NT) = 32 with steady-state pulses (SS) = 2; the data was processed with line-broadening (LB and LB2) = 0.1 Hz in both t_1 and t_2, respectively; the data points in t_1 were zero-filled to 2048 points prior to Fourier transformation. The data acquisition parameters used for **5** were the same as that for **3** with the following exceptions: AT = 332 ms; SW = 3085.5 Hz; the processing parameters for **5** were the same as those used for **3**.

Phase-sensitive NOESY. — The data-acquisition parameters for **3** were the same as for the DQF-COSY for **3** data except for the following: sequence, D1–(90)–t_1–(90)–MIX–(90)–acquire (t_2); D1 = 15 s; mixing time (MIX) = 1.0 s. The phase-sensitive NOESY acquisition parameters for **5** were the same as for the corresponding DQF-COSY data except for the sequence. The data processing for both data sets was the same as for the dQF-COSY data sets, respectively. The DQF-COSY and NOESY results for both **3** and **5** are summarized in Figs. 1–4.

Proton–carbon-13 heteronuclear shift correlation (HETCOR). — The acquisition parameters for the experiment for **3** and for **5** are as follows: sequence D1–(90)(H)–t_1/2-BIRD pulse (H,C)–t_1/2–(90)(H,C)–acquire (t_2); D1 = 2 s; J1XH = 140 Hz (average value for for direct 1-bond correlation); PW90(H) or PP = 20 μs; PW90(C) = 14.8 μs; the carbon-13 SW for **3** was 16666.7 Hz in F_2 and for **5** was 13315.6 Hz in F_2. The proton SW for **3** and **5** was 2976.2 Hz (F_1) and 3085.5 Hz

(F_1), respectively. The AT of the HETCOR experiments for **3** and **5** was 123 ms (NP = 4096) and 77 ms (NP = 2048), with NT = 128 and 256, and NI = 128 and 256, respectively. The data points in t_1 were zero-filled to 512 and 1024 points, respectively for **3** and **5**, prior to Fourier transformation using pseudo-echo weighting in both frequency domains with absolute value (AV) display. Figs. 5 and 6 summarize the HETCOR results for **3** and **5**.

Molecular modeling. — Molecular modeling studies were carried out on **3**, **5**, **6**, and **7** with a view to determine their energetically favored conformations and to determine if the conformational characteristics of the low-energy minima correlate with the NMR derived distances (NOE) and torsion angles (vicinal proton–proton coupling constants). In order to achieve this, it is necessary to exhaustively investigate the conformations possible for these compounds and to determine which low-energy conformations fit the experimental data. In particular, the flexibility due to the pseudorotation in the five-membered rings deserves attention.

Preliminary models of **3**, **5**, and **7** were built using the computer graphics package MacroModel[18] and refined using a combination of steepest descent, block-diagonalized Newton–Raphson and full-matrix Newton–Raphson minimization techniques. Throughout the study the force field used was the MacroModel version of MM2. The preliminary models were refined with a dielectric value of 1.0.

In the next phase of computations, the pseudorotational variants of the fused bicyclic component in these molecules were generated by constraining the ring torsions to specific values (Table VII). In **5** and **7**, there are 38 distinct pseudorotational states, since both rings are saturated and hindered rotations are possible about all nine bonds. In **3**, only 20 pseudorotational states are possible since the C-3 carbon is sp^2 hybridized, leading to a rigid five-membered ring. The ring torsions were constrained to the sets of values in Table VII using a cosine-type penalty function with a constraint weight of 1000 kcal/mol. The resultant minimized models had ring torsions within 0.1° of the desired values.

Corresponding to each of the 38 refined models for **5**, multiple conformations were generated as a function of (*a*) the pseudorotation of the 5,6-isopropylidene ring and (*b*) rotations about the C-3–C-3′ and C-4–C-5 bonds. In the case of rotations, conformations were generated at intervals of 60°. Thus the starting number of conformations for **5** was 27360. A number of these were eliminated even before energy refinement by van der Waals criteria[17]. Conformations free of short contacts were then refined using the Batchmin module of MacroModel on the 16-node Intel Hypercube parallel machine. Multiple conformations were generated for **3** and **7** in the same manner. The number of starting conformations for **3** and **7** were 2400 and 4560, respectively, since in the former no rotation about the substituent at C-3 is possible and in the latter there is no bulky substituent at C-3.

To ensure that all possible low-energy models were obtained, Batchmin calculations were carried out in two stages. In the first stage, the starting conformations

TABLE VII

Torsion angles used in the generation of twenty puckering forms of a saturated five-membered ring defined by atoms A1, A2, A3, A4, and A5 (a) and thirty eight puckering forms of a saturated perhydropentalene system defined by atoms A1, A2, A3, A4, A5, A6, A7, and A8 with the first five atoms forming one ring and (A4, A5, A6, A7, and A8) forming the other ring (b). Five torsions $\sigma 1$(A5-A1-A2-A3), $\sigma 2$(A1-A2-A3-A4), $\sigma 3$(A2-A3-A4-A5), $\sigma 4$(A2-A4-A5-A1), and $\sigma 5$(A4-A5-A1-A2) characterize the five-membered ring, while nine torsions $\sigma 1$(A5-A1-A2-A3), $\sigma 2$(A1-A2-A3-A4), $\sigma 3$(A2-A3-A4-A5), $\sigma 4$(A2-A4-A5-A1), $\sigma 5$(A4-A5-A1-A2), $\sigma 6$(A1-A5-A6-A7), $\sigma 7$(A5-A6-A7-A8), $\sigma 8$(A6-A7-A8-A4), and $\sigma 9$(A7-A8-A4-A3) characterize the perhydropentalenes

(a)

$\sigma 1$	$\sigma 2$	$\sigma 3$	$\sigma 4$	$\sigma 5$
45.0000	−36.4058	13.9058	13.9058	−36.4058
42.7975	−42.7975	26.4503	0.0	−26.4503
36.4058	−45.0000	36.4058	−13.9058	−13.9058
26.4503	−42.7975	42.7975	−26.4503	0.0
13.9058	−36.4058	45.0000	−36.4058	13.9058
0.0	−26.4503	42.7975	−42.7975	26.4503
−13.9058	−13.9058	36.4058	−45.0000	36.4058
−26.4503	0.0	26.4503	−42.7975	42.7975
−36.4058	13.9058	13.9058	−36.4058	45.0000
−42.7975	26.4503	0.0	−26.4503	42.7975
−45.0000	36.4058	−13.9058	−13.9058	36.4058
−42.7975	42.7975	−26.4503	0.0	26.4503
−36.4058	45.0000	−36.4058	13.9058	13.9058
−26.4503	42.7975	−42.7975	26.4503	0.0
−13.9058	36.4058	−45.0000	36.4058	−13.9058
0.0	26.4503	−42.7975	42.7975	−26.4503
13.9058	13.9058	−36.4058	45.0000	−36.4058
26.4503	0.0	−26.4503	42.7975	−42.7975
36.4058	−13.9058	−13.9058	36.4058	−45.0000
42.7975	−26.4503	0.0	26.4503	−42.7975

(b)

$\sigma 1$	$\sigma 2$	$\sigma 3$	$\sigma 4$	$\sigma 5$	$\sigma 6$	$\sigma 7$	$\sigma 8$	$\sigma 9$
−35.6	44.0	−35.6	13.6	13.6	44.0	−35.6	13.6	13.6
−35.6	44.0	−35.6	13.6	13.6	13.6	13.6	−35.6	44.0
−25.9	41.8	−41.8	25.9	0.0	41.8	−41.8	25.9	0.0
−25.9	41.8	−41.8	25.9	0.0	0.0	25.9	−41.8	41.8
−13.6	35.6	−44.0	35.6	−13.6	35.6	−44.0	35.6	−13.6
−13.6	35.6	−44.0	35.6	−13.6	−13.6	35.6	−44.0	35.6
0.0	25.9	−41.8	41.8	−25.9	25.9	−41.8	41.8	−25.9
0.0	25.9	−41.8	41.8	−25.9	−25.9	41.8	−41.8	25.9
13.6	13.6	−35.6	44.0	−35.6	13.6	−35.6	44.0	−35.6
13.6	13.6	−35.6	44.0	−35.6	−35.6	44.0	−35.6	13.6
25.9	0.0	−25.9	41.8	−41.8	0.0	−25.9	41.8	−41.8
25.9	0.0	−25.9	41.8	−41.8	−41.8	41.8	−25.9	0.0
35.6	−13.6	−13.6	35.6	−44.0	−13.6	−13.6	35.6	−44.0
35.6	−13.6	−13.6	35.6	−44.0	−44.0	35.6	−13.6	−13.6
41.8	−25.9	0.0	25.9	−41.8	−25.9	0.0	25.9	−41.8
41.8	−25.9	0.0	25.9	−41.8	−41.8	25.9	0.0	−25.9
44.0	−35.6	13.6	13.6	−35.6	−35.6	13.6	13.6	−35.6
41.8	−41.8	25.9	0.0	−25.9	−41.8	25.9	0.0	−25.9
41.8	−41.8	25.9	0.0	−25.9	−25.9	0.0	25.9	−41.8

TABLE VII (continued)

(b)

σ1	σ2	σ3	σ4	σ5	σ6	σ7	σ8	σ9
35.6	−44.0	35.6	−13.6	−13.6	−44.0	35.6	−13.6	−13.6
35.6	−44.0	35.6	−13.6	−13.6	−13.6	−13.6	35.6	−44.0
25.9	−41.8	41.8	−25.9	0.0	−41.8	41.8	−25.9	0.0
25.9	−41.8	41.8	−25.9	0.0	0.0	−25.9	41.8	−41.8
13.6	−35.6	44.0	−35.6	13.6	−35.6	44.0	−35.6	13.6
13.6	−35.6	44.0	−35.6	13.6	13.6	−35.6	44.0	−35.6
0.0	−25.9	41.8	−41.8	25.9	−25.9	41.8	−41.8	25.9
0.0	−25.9	41.8	−41.8	25.9	25.9	−41.8	41.8	−25.9
−13.6	−13.6	35.6	−44.0	35.6	−13.6	35.6	−44.0	35.6
−13.6	−13.6	35.6	−44.0	35.6	35.6	−44.0	35.6	−13.6
−25.9	0.0	25.9	−41.8	41.8	0.0	25.9	−41.8	41.8
−25.9	0.0	25.9	−41.8	41.8	41.8	−41.8	25.9	0.0
−35.6	13.6	13.6	−35.6	44.0	13.6	13.6	−35.6	44.0
−35.6	13.6	13.6	−35.6	44.0	44.0	−35.6	13.6	13.6
−41.8	25.9	0.0	−25.9	41.8	25.9	0.0	−25.9	41.8
−41.8	25.9	0.0	−25.9	41.8	41.8	−25.9	0.0	25.9
−44.0	35.6	−13.6	−13.6	35.6	35.6	−13.6	−13.6	35.6
−41.8	41.8	−25.9	0.0	25.9	41.8	−25.9	0.0	25.9
−41.8	41.8	−25.9	0.0	25.9	25.9	0.0	−25.9	41.8

were refined with a dielectric constant of 1.0 (see below) by holding the ring geometries fixed using the FIXT option*. Block-diagonalized Newton-Raphson minimization technique was used and the models were refined until a gradient of 0.005 kcal/mol/Å was achieved. Conformations higher than 7 kcal/mol in energy relative to the global minimum were eliminated from further consideration.

In the second stage, the resultant reduced set of conformations for each molecule was then subjected to full minimizations in which no constraints were imposed on any conformational parameters. These calculations were done at two sets of dielectric constants, 1.0 and 10.0. In the MM2 force field, electrostatic interactions are represented by Coulomb's law and are typically evaluated at a dielectric constant of 1.0. This simplistic representation tends to overemphasize electrostatic effects, particularly when a molecule consists of groups which can form intramolecular hydrogen bonds or ionic interactions. Consequently, interactions with the solvent environment tend to be underemphasized and this may result in "solution-bound conformations" being missed in the conformational analysis. In order to ascertain the inclusion of such conformations in our analysis, we also carried out the molecular mechanics calculations with a dielectric constant of 10.0. It should be pointed out that a number of dielectric models have been used in the literature[19] to correct for the overemphasis of electrostatic effects.

* The MacroModel program (version 2.5) was modified by Dr. Dale Spangler, Drug Design of Searle Research and Development, to incorporate the option of keeping torsion angles fixed (FIXT) during energy optimizations in the Batchmin module.

However, there exists no unique model to achieve this. As such, our choice of a dielectric constant of 10.0 is not unreasonable in that the resultant models were qualitatively indistinguishable from those obtained with a dielectric constant of 1.0.

Structures were eliminated from consideration not only on energy criteria (see above), but also on the basis of uniqueness. Two structures are considered unique if the root-mean-square deviation of all the ring atoms and the atoms in the bulky substituents, other than methyl carbons, was not > 0.3 Å. In the final sets, structurally unique low-energy minima were arranged in an ascending order of energy. These were then viewed and analyzed graphically using SYBYL*.

For the sake of completeness, energy calculations were also performed on **6**, wherein a methyl group was substituted for the cyanomethyl moiety in **5**. The unique energy minima of **5** were chosen as the starting point for the molecular modeling of **6**. Energies were minimized as described above using only a dielectric constant of 1.0.

ACKNOWLEDGMENTS

Microanalytical results, mass spectra and IR spectra were obtained by the Physical Methodology Department at Searle. We acknowledge Ms. Lilian Garcia for her assistance in obtaining the NMR data described here. Catalytic hydrogenation was performed by the Hydrogenation Group of Searle. We thank Professor G.W.J. Fleet and Mr. D.R. Witty (Oxford University) for sharing their PCC oxidation conditions with us. We are grateful to Dr. Dale Spangler of Drug Design and Mr. Dan Volocyk of SMIS for their intense efforts in the port of the Batchmin module in MacroModel to the parallel computing environment of Intel Hypercube together with the development of a user-friendly interface. The authors acknowledge Ms. Marge Hille, Ms. Eden Mante, Ms. Dorothy Ryno, Mr. Frank Yang and Ms. Teresa Yim of Searle Information Services for their assistance.

REFERENCES

1 (a) S. Hanessian and G. Rancourt, *Pure Appl. Chem.*, 49 (1977) 1201–1214; (b) S. Hanessian, *Acc. Chem. Res.*, 12 (1979) 159–165; (c) P.J. Garegg, *Pure Appl. Chem.*, 56 (1984) 845–858; (d) T.D. Inch, *Tetrahedron*, 40 (1984) 3161–3213; (e) T. Suami, *Pure Appl. Chem.*, 59 (1987) 1509–1520.

2 P. Daïs and A.S. Perlin, *Carbohydr. Res.*, 146 (1986) 177–191.

3 (a) A. Rosenthal and D.A. Baker, *J. Org. Chem.*, 38 (1973) 193–197; (b) D.C. Baker, D. Horton, and C.G. Tindall, Jr., *Methods Carbohydr. Chem.*, 7 (1976) 3–6.

4 (a) J.M.J. Tronchet, J.-M. Bourgeois, J.-M. Chalet, R. Graf, R. Gurny, and J. Tronchet, *Helv. Chim. Acta*, 54 (1971) 687–694; (b) J.M.J. Tronchet and J.-M. Bourgeois, *ibid.*, 55 (1972) 2820–2827; (c) J.M.J. Tronchet and J.-M. Bourgeois, *Carbohydr. Res.*, 29 (1973) 373–385; (d) See ref. 3a.

5 (a) U. Piantini, O.W. Sorensen, and N.N. Ernst, *J. Am. Chem. Soc.*, 104 (1982) 6800–6801; (b) G.E. Martin and A.S. Zektzer, *Two-Dimensional NMR Methods for Establishing Molecular Connectivity: A*

* SYBYL version 5.32. Molecular modeling software developed and released by Tripos Associates, Inc. Copyright 1986, 1989, and 1990.

Chemist's Guide to Experiment Selection, Performance, and Interpretation, VCH, New York, 1988, pp. 58–161.
6 (a) D.J. States, R.A. Haberkorn, and D.J. Ruben, *J. Magn. Reson.*, 48 (1982) 286–292; (b) D. Neuhaus and M. Williamson, *The Nuclear Overhauser Effect in Stereochemical and Conformational Analysis*, VCH, New York, 1989.
7 S.L. Patt and J.N. Shoolery, *J. Magn. Reson.*, 46 (1982) 535–539.
8 (a) A. Bax and G.A. Morris, *J. Magn. Reson.*, 42 (1981) 501–505; (b) A. Bax, *ibid.*, 53 (1983) 517–520.
9 (a) J.G. Buchanan, A.R. Edgar, D.I. Rawson, P. Shahidi, and R.H. Wightman, *Carbonhydr. Res.*, 100 (1982) 75–86; (b) J.G. Buchanan, M.E. Chacon-Fuertes, A.R. Edgar, S.J. Moorhouse, D.I. Rawson, and R.H. Wightman, *Tetrahedron Lett.*, 21 (1980) 1793–1796; (c) G. Aslani-Shotorbani, J.G. Buchanan, A.R. Edgar, D. Henderson, and P. Shahidi, *ibid.*, 21 (180) 1791–1792.
10 K. Bock and C. Pedersen, *Adv. Carbohydr. Chem. Biochem.*, 41 (1983) 27–66.
11 M. Karplus, *J. Am. Chem. Soc.*, 85 (1963) 2870–2871.
12 C.A.G. Haasnoot, F.A.A.M. de Leeuw, and C. Altona, *Tetrahedron*, 36 (1980) 2783–2792.
13 L.D. Hall, S.A. Black, K.N. Slessor, and A.S. Tracey, *Can. J. Chem.*, 50 (1972) 1912–1924.
14 A. Rosenthal and M. Sprinzl, *Can. J. Chem.*, 47 (1969) 3941–3946.
15 T.M. Calub, A.L. Waterhouse, and A.D. French, *Carbohydr. Res.*, 207 (1990) 221–235.
16 D.A. Pearlman and S.H. Kim, *J. Biomolec. Struct. Dyn.*, 3 (1985) 85–128, and references therein.
17 D.C. Lankin, S.T. Nugent, and S.N. Rao, in preparation.
18 F. Mohamadi, N.G.J. Richards, W.C. Guida, R. Liskamp, M. Lipton, C. Caufield, G. Chang, T. Hendrickson, and W.C. Still, *J. Comput. Chem.*, 11 (1990) 440–467.
19 (a) P.A. Kollman, P.K. Weiner, and A. Dearing, *Biopolymers*, 20 (1981) 2583–2621; (b) P.A. Kollman, J.W. Keepers, and P.K. Weiner, *ibid.*, 21 (1982) 2345–2376; (c) S.N. Rao and V. Sasisekharan, *Ind. J. Biochem. Biophys.*, 18 (9181) 303–310.